Where is the 'Jennifer Aniston neuron'?

Dorian Aur[1], Peter N Steinmetz[2]
[1]Dept. of Comparative Medicine, Stanford University, Palo Alto, CA
[2]Dept. of Neurology and Neurosurgery, Barrow Neurological Institute, Phoenix, AZ

Abstract: It is generally believed that spike timing features (firing rate, ISI) are the main characteristics that can be related to neural code. Contrary to this common belief, spike directivity, a new measure that quantifies transient charge density dynamics within action potentials (APs) provides better results in discriminating different categories of visual object recognition. Specifically, intracranial recordings from medial temporal lobe (MTL) of epileptic patients have been analyzed using firing rate, interspike intervals and spike directivity. A comparative statistical analysis of the same spikes from four selected neurons shows that electrical micro-mapped features in neurons display higher separability to input images compared to spike timing features. If the observation vector include data from all 4 neurons then the comparative analysis shows a highly significant separation between categories for spike directivity ($p=0.0023$) and does not display separability for ISI ($p=0.3768$) and firing rate ($p=0.5492$). The presence of electrical micro-maps within APs suggests the existence of an intrinsic "neural code" where information regarding input images is electrically written/coded and read/decoded during AP propagation in the neuron. The occurrence of electrical micro-maps within APs reflects information communication and computation in analyzed neuron within a millisecond-level time domain of AP occurrence. This existence of a "lower level" of coding where information is processed within neurons raises questions regarding the richness and reliability of models that constrain neural code to spike timing features. Additionally, this phenomenon that occurs within APs may provide a step forward in understanding the fundamental gap between molecular description, information processing and neuronal function. Importantly, this paper confirms a new paradigm regarding neural code where information processing, computation and memory formation in the brain can be explained in terms of dynamics and interaction of electric charges.

Key words: neural code, firing rate, interspike interval, spike directivity

Introduction

One important function of the brain is to represent and transform information received from sensory inputs. Large populations of neurons are commonly involved in information processing in the nervous system. How this information is processed by every cell in the network and how information is then integrated in ensembles of neurons remained unexplained even though there is a huge amount of work in collecting and analyzing data. For more than seven decades the analysis of neuronal activity has been reduced to firing rate analysis. Temporal modulation, changes depending on stimuli inputs have been observed in earlier analyses as alterations of the frequency of action potentials occurrences (Adrian, 1928). Therefore, the main idea of recordings and current analyses in neuroscience is to analyze temporal patterns. More recently

[1] To whom correspondence should be addressed. E-mail: DorianAur@gmail.com

besides firing frequency data, interspike interval (ISI) has been assumed to better characterize stimuli inputs and provide an accurate representation of distributed neural code (Gerstner and Kistler, 2002). The classic coding model highlights the importance of temporal patterns in large-scale brain networks (Honey et al., 2007; Felleman and Van Essen, 1991; Softky and Koch, 1993; Abbott et al., 1997; Shadlen and Newsome, 1998).

Quiroga et al., (Quiroga et al. 2005) showed that single MTL neurons fire selectively in response to a particular face, animal, object or scene since single neurons may encode features of particular objects. In particular selected neurons show selective, invariant, and explicit responses to a set of images of Jennifer Aniston. The neuronal activity in the temporal lobe is related to visual recognition of different objects (Liu et al., 2009). It is already known that hippocampal formation encodes episodic memories and is involved on conscious remembering (Shirvalkar, et al., 2009). Almost always these responses in single units outlast stimulus presentation and can be associated with conscious recognition (Quiroga et al., 2008). Additionally, Quiroga et al., (Quiroga et al., 2009) tried to explain how the brain recognizes highly variable pictures as the same percept. In order to evoke selective responses to presented images attention is required (Steinmetz, 2009). We know from Kreiman, et al. that the same neurons are activated during vision and visual imagery and that firing rate is supposed to be able to separate between various categories (Kreiman et al., 2000).

Based on estimated firing rate all these analyses do not explicitly show any relationship with intrinsic cellular processes that may occur during visual information processing and several further questions were raised in medical and scientific community. How are categories identified, classified and remembered in these neurons? Are there network modules dedicated to face perception? What is the relationship between temporal patterns (firing rate, ISI) and memory formation?
In this paper we will try to provide some answers to these important questions using ‘spike directivity’ a measure that captures electrical features specific to cell neurophysiology during AP propagation.

Spike Directivity

Contrary to common belief action potentials are not uniform (stereotyped) pulses of electricity. It is likely that changes in synaptic and non-synaptic inputs that generate APs occurrence causes alterations of intracellular features and determines preferential dynamic activation of ion channels, different dendritic currents which provides small changes in the shapes of action potentials (Gold et al, 2006, Aur et al., 2005; Aur and Jog, 2006; Aur and Jog, 2010). Since intrinsic electrical communication and information processing during AP occurrence is hidden, computational techniques can be used to extract information from small changes in the APs waveforms. If a reference in space is considered (e.g. one tip of tetrodes) these spatial changes in charge density can be approximated with a vector called spike directivity. Spike directivity (SD) characterizes the distribution of electric events during AP propagation in an analyzed neuron (Aur et al., 2005). Spike directivity is a vector that can be computed for every AP and displays the preferred direction of electric propagation. While firing rate and ISI investigations require sufficient numbers of spikes and extensive statistical analyses in order to assess neural activity, spike directivity can be computed for every recorded spike and provides information regarding

electrical processes developed in the neuron. Previous in vivo recordings performed in freely behaving rodents during a T-maze procedural learning task and the analysis of spike directivity in selected expert neurons demonstrated that neural activity can be directly related with the semantics of behavior. Such analyses performed with tetrodes proved that besides temporal patterns (spike timing changes) there are other important electric features intrinsic to cell neurophysiology which are highly modulated during T-maze procedural learning task (Aur and Jog, 2007a; Aur and Jog, 2007b). Relevant changes in spatial distribution of charge density within generated action potentials recorded from single neurons make spikes non-stereotype events that carry meaningful information regarding behavior not necessarily in a temporal domain.

In this paper we would like to compare different methods of analysis in terms of their relevance in separating categories. Therefore in a selected group of cells that responded to presented images the analysis of firing rate, interspike interval and spike directivity are compared in order to respond to several questions outlined above.

Methods

Patients with pharmacologically intractable epilepsy have been implanted as described in (Kreiman et al., 2000) with depth electrodes to detect the area of seizure onset. The placement of the depth electrodes in the MTL followed limited clinical requirements. Images of faces, animals, and landscapes were presented for 1 s in pseudo-random order on a laptop computer in multiple recording sessions, six times each. During all sessions patients were asked to indicate whether a human face was presented. All patients were able to identify human faces with the error rate less than 1%. Majority of these neurons responded to several presented images. Spike detection and sorting were performed and applied to recorded data using well established algorithms. The raw cross-correlations indicate the presence of similar AP recorded from the same set of neurons. Since the same APs were detected in at least four electrodes a 'tetrode' framework has been used for analysis.

First, an automated unsupervised classification of multidimensional data in the tetrode setup was used (KlustaKwik (KK), Harris K. D. et al., Rutgers University). The default values of KlustaKwik from Mclust along with energy features are used. Pre-clustered spikes with similar means were merged together and from 17 clusters only 9 clusters were further considered, about 2000 spikes. The events/neurons with small amplitudes (max values less than <0.1 mV) were not considered and also one cluster with very high amplitudes was not further included. Smaller amplitudes of AP are not included since the noise may impact the spike directivity (SD) outcome. This procedure was followed by manual selection of spikes. The final result shows four well separated clusters with signal amplitudes >0.1 mV which provided four neurons (N1, N2, N3 and N4) with their action potentials (APs) that have been further analyzed (Supplementary Figure 18). The peristimulus time histogram (PSTH) is represented for each category and all four analyzed neurons (see Suplementary Figure 13 to Figure 16) showing the times at which the neurons fire. The presence of a refractory period for the single units has been checked (less 1% spikes within <3-ms ISI). The maximum values for the means of amplitudes provide the difference between four channels in a tetrode like configuration where about 550 spikes are generated by 4 neurons, (see Table 2 and Figure 17, Supplementary Material). For each clustered spike we computed spike directivity using the algorithm presented in (Aur et al.,2005) (see also Appendix1).

Hypothesis 1: The firing rate is an accurate measure of information processed by neurons during object presentation.

The set of features f_i varies from image to image, however it is expected that objects from a certain category share similar features. The set of features refer to relevant attributes of presented images that may include semantic aspects or any other characteristics. Usually the neural response is measured based on estimated firing rate. Given a set of features $f_i \in F$ the neuron transforms (maps) this set of features in series of action potentials (APs) in such way that $h_{firing_i} \in H_F$ represent the image features f_i:

$$F \overset{T_F}{\rightarrow} H_F \qquad (1)$$

T_F is the transformation from image feature to ISI.

Hypothesis 2 The interspike interval distribution is an accurate measure of information processed by neurons during object presentation. Probability density of ISI can be considered as a measure of neural activity that embeds more information than the firing rate measures (Gerstner and Kistler, 2002). Therefore, given the same set of features $f_i \in F$ the neuron transforms (maps) this set of features in interspike interval data in such a way that $h_{ISI\,i} \in H_{ISI}$ represents image features f_i

$$F \overset{T_{ISI}}{\rightarrow} H_{ISI} \qquad (2)$$

T_{ISI} is the transformation from image feature to ISI.

*Hypothesis 3: S*pike directivity provides an accurate measure of information processed by neurons during object presentation. It is considered that neurons process and extract features from presented images, therefore given a set of features $f_i \in F$ the neuron transforms (maps) these features in electrical patterns in such a way that $h(x_i, y_i, z_i) \in H_{SD}$ represents f_i

$$F \overset{T_{SD}}{\rightarrow} H_{SD} \qquad (3)$$

where $h(x_i, y_i, z_i)$ represents the distribution of electrical charges in Cartesian coordinates(x_i, y_i, z_i) and T_{SD} is the transformation from object feature into a distribution of electric charges. Since spike directivity characterizes the distribution of electrical charges, here, the main hypothesis is that there is a relationship between object presentation and the presence of electrical patterns (micro-maps) during action potential propagation. The existence of patterns of activation (micro-maps) determined by different spatial charge densities has been recently evidenced in APs (Aur and Jog, 2006; Aur and Jog, 2007).

In order to test above hypotheses, the activity of a relatively small subset of neurons from MTL that responded to a series of presented images is analyzed. The main idea is to test statistical significance of these hypotheses in providing information regarding object category. Since there are only three categories of presented images, their specific characteristics can be formalized using a set description which includes all five presented images for faces f^{FACES}, five presented images for animals f^{ANIM} and five presented images for landscapes f^{LAND} (see Appendix 2)

Specifically the presentation of each image category generates in the output space the following sets for faces h^{FACES}, for animals h^{ANIM} and h^{LAND} for landscapes. This output will be different

depending which characteristics (firing rate, ISI or SD) are selected in the analysis. The mean firing rate can be obtained by counting spikes N_{sp} that appeared divided by the length of observation period, T.

$$h_{firing} = \frac{N_{sp}(T)}{T} \qquad \textbf{(4)}$$

Since images are repeatedly presented, then an estimation of firing rate can be obtained if this value is averaged. The mean firing rate response to a picture is computed as the median number of spikes across trials between 200 and 2,000 ms after stimulus onset. The result is a projection of input features (image characteristics) in a temporal firing rate domain h_{FR}^{FACES} for faces, h_{FR}^{ANIM} for animals and h_{FR}^{LAND} for landscapes. Similar characteristics are mapped in interspike temporal domain. The probability density estimates of interspike interval are obtained using a kernel density estimator and generate the following characteristics h_{ISI}^{FACES} for faces, h_{ISI}^{ANIM} for animals and h_{ISI}^{LAND} for landscapes.

As presented above the propagation of electric potential and the occurrence of electrical patterns during AP propagation can be characterized by spike directivity. The corresponding output features $h_{SDi} \in H_{SD}$ can be determined by computing spike directivity and represented as points on a sphere :

$$S^2 = \{r \in R^3 : \| r \| = 1\} \qquad \textbf{(5)}$$

where spike directivity arrow head points on the 2-sphere surface (Fig 1) .

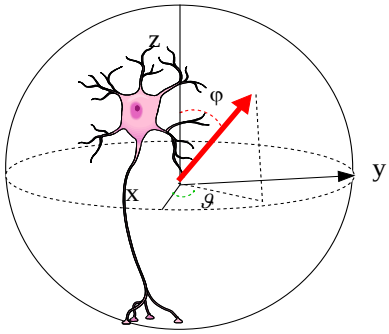

Figure 1: Schematic representation of a scaled neuron included in a unit sphere. Spike directivity vector in red color is a reflection of spatial distribution of electric charges during AP propagation. The spike directivity arrow head points on the 2-sphere surface. In a spherical coordinate system the angles θ and φ characterize the orientation of the spike directivity vector (θ values range from 0-2 π while φ values range from 0- π).

In order to analyze the distribution the electrical features represented by the head of arrows the representation is transformed from three-dimensional Cartesian coordinates (x_i,y_i,z_i) into spherical coordinates θ_i and φ_i where :

$$\theta_i = a\tan(\frac{y_i}{x_i}) \qquad \textbf{(6)}$$

and:

$$\varphi_i = a\tan(\frac{z_i}{\sqrt{x_i^2 + y_i^2}}) \qquad \textbf{(7)}$$

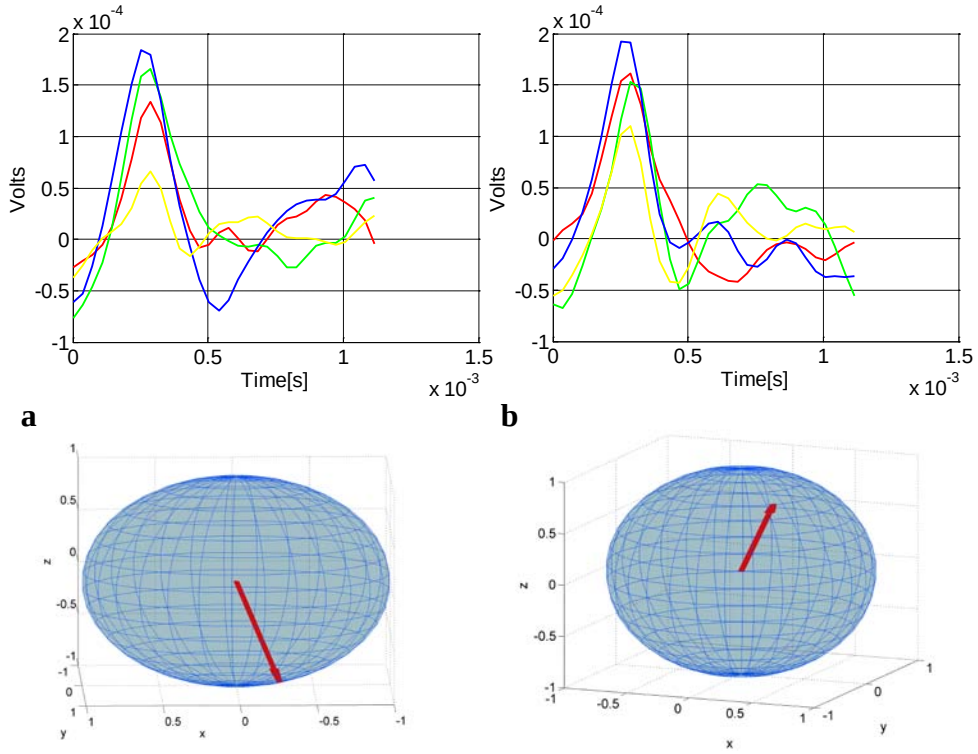

Figure 2: Two different spikes from the same neuron recorded from four electrodes (in blue, red, green and yellow) display two different spike directivities. Differences in recorded voltages within these two spikes represented in a and b are reflected in corresponding changes in spike directivity in c and d. The head of the arrow points on a sphere with radius one ($\| r \| = 1$)

a, Four recorded waveforms and their corresponding spike directivity represented in the north hemisphere **c.**
b, Four recorded waveforms and their corresponding spike directivity represented in the south hemisphere **d.**

The density of mapped features (only θ_i angle is considered) can be estimated using a kernel density estimator:

$$\hat{h}(\theta) = \frac{1}{ns}\sum_{i=1}^{n}\left(\frac{K(\theta-\theta_i)}{s}\right) \qquad \textbf{(8)}$$

where K is a Gaussian kernel and s is the smoothing parameter (Terrell and Scott, 1992). These electric characteristics on the sphere are representation of features h_{SD}^{FACES} for faces, h_{SD}^{ANIM} for animals and h_{SD}^{LAND} for landscapes that occur in these neurons when images from the above categories are presented.

Results: A Comparative Analysis

The representation of spike directivity displays in an explicit topographic manner the relationship with encoded categories (Figure 3). One way ANOVA statistics is used to determine if these

characteristics of faces h^{FACES} animals h^{ANIM} and landscapes h^{LAND} are well separated. Similar analysis is performed for probability distributions of firing rate and ISI and then compared.

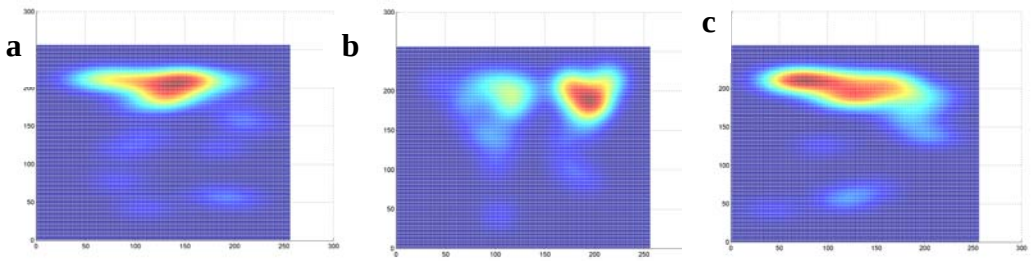

Figure 3: Representation of spike directivity characteristics projected on the north hemisphere across θ (abscissa[deg]) and φ angles displays in a topographic manner the relationship with encoded categories (**a**) for faces, h_{SD}^{FACES} (**b**) for animals h_{SD}^{ANIM} and (**c**) for landscapes h_{SD}^{LAND} in selected neuron (N_1)

The analyzed neurons responded primarily to all different images (see the peristimulus time histogram in supplementary Figure 13 to Figure 16). The estimated F-ratio and p-values summarize the result of comparative statistical analysis (Table 1). Larger values of F-ratio show that the variation among group means is unlikely to occur by chance. In the first two neurons one way ANOVA statistics of firing rate characteristics does not provide any separation between categories (p-values >0.1) N_1: p_{FR}=0.678, N_2: p_{FR}=0.248). However, the observed difference is significant (p_{FR}<0.05) in neuron N_4: p_{FR}=0.0261 and marginally significant (p_{FR}<0.1) in neuron N_3: p_{FR}=0.09 (supplementary Figure 6 to Figure 9). Similar analysis carried on using probability density of ISI displays highly significant category separability ($p_{ISI} < 0.01$) in two neurons (N_2: p_{ISI}=0.0008; N_3: p_{ISI} =9.9749e-007) and does not provide any separation in other two neurons (N_1: p_{ISI} =0.3196; N_4: p_{ISI} =0.1723) (supplementary Figure 12). Interestingly the neuron where firing rate shows this high separability between ISI characteristics N_2: p_{ISI}=0.0008 is the one where the firing rate does not provide any separation (N_2: p_{FR}=0.248). Additionally the difference is significant in neuron N_4: p_{FR}=0.0261 and does not display separability if ISI is analyzed in N_4: p_{ISI} =0.1723.

	Firing rate		ISI		SD	
	p	F	p	F	p	F
N1	0.678	0.4	0.3196	1.15	0.028	3.62
N2	0.248	1.57	0.0008	7.3	0.0012	6.87
N3	0.09	2.95	9.9749e-007	14.48	0.065	2.75
N4	0.0261	5.01	0.1723	1.77	0.011	4.57

Table 1

However, one way ANOVA statistics of probability density function of the θ angle shows that electric characteristics generated during AP propagation in these neurons significantly separate

a

these categories with p-values: N_1: p_{SD}^N =0.028, N_2: p_{SD}^N =0.0012; N_4: p_{SD}^N =0.011 and the difference is marginally significant in one neuron (N_3: p_{SD}^N =0.065<0.1) (supplementary Figure 10 and Figure 11).

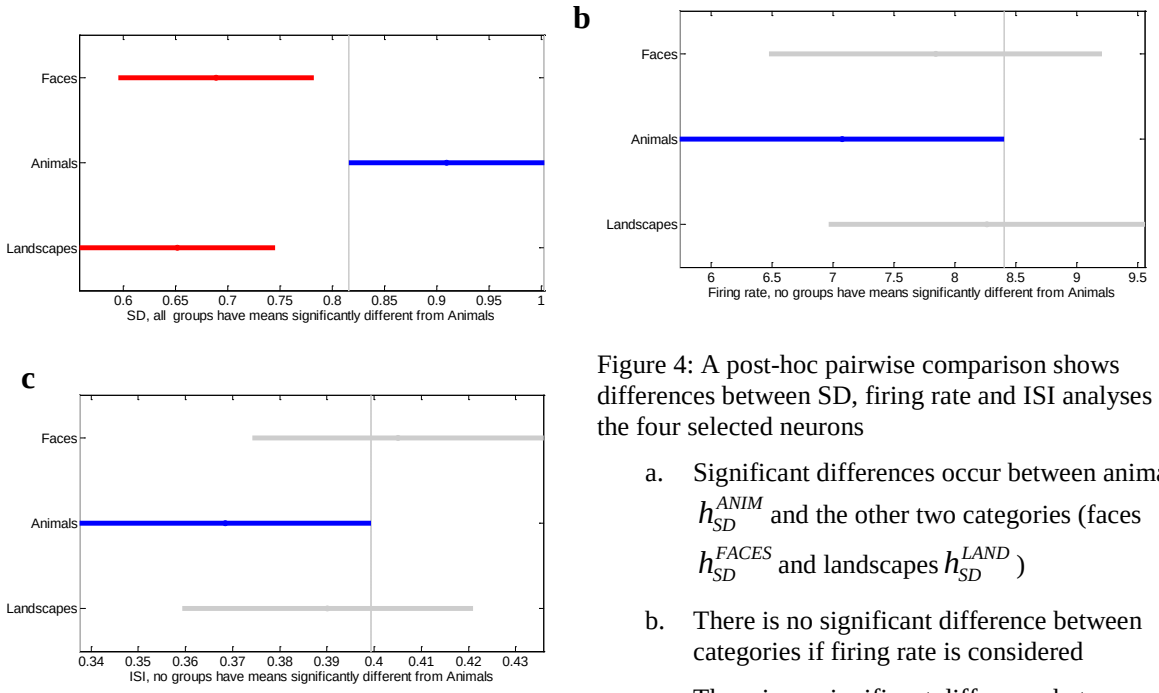

Figure 4: A post-hoc pairwise comparison shows differences between SD, firing rate and ISI analyses in the four selected neurons

a. Significant differences occur between animals h_{SD}^{ANIM} and the other two categories (faces h_{SD}^{FACES} and landscapes h_{SD}^{LAND})
b. There is no significant difference between categories if firing rate is considered
c. There is no significant difference between categories if ISI is considered.

If the observation vector include data from all 4 neurons then the comparative analysis shows a highly significant separation between categories for spike directivity (F=6.09 p=0.0023) and does not display separability for ISI (F=0.98 p=0.3768) and firing rate (F=0.61 p=0.5492) (see supplementary Figure 17, a-c). A post-hoc pairwise comparison shows that significant difference is relevant between animals and the other groups (faces and landscapes) while firing rate and ISI do not provide a significant difference between the groups (Figure 4)

Discussion

Since all four neurons responded to analyzed categories it is likely that information regarding presented images is distributed coded/decoded in a large number of neurons. In these four selected neurons spike directivity analysis outperforms firing rate and ISI outcome in relating neuronal activity with object presentation. Firing rate and ISI do not always display a statistical significant relationship with encoded/decoded object categories. Even though spike directivities are related to inputs that generate APs onset and temporal variability it is likely that the presence of these patterns that reflect different charge densities within spikes is complimentary to APs occurrence in time. Therefore, in these patterns additional information is included that cannot be extracted from ISI or firing rate analyses. This phenomenon suggests that during AP propagation, information regarding presented objects can be carried and embedded in electrical patterns within spikes. Clearly, different propagation of action potentials can have implications

and consequences for synaptic changes and signal processing within the downstream cells. However, the communication of information and information processing can be seen as two distinct phenomena, in general information communication reflects just a start-up part of computation. When and where the synaptic communication of information between cells occurs is important, however, the synaptic transmission reveals only the modulated transfer of information between neurons and does not reflect the entire process of computation which seems mainly to take place in the cell. Within every neuron information communication and processing are close related. The observed changes of electrical patterns show how information is processed and communicated endogenously within the neuron and points to a more complex non-Turing model of computation required to describe neuronal activity (Aur and Jog, 2010).

The observed transient charge density dynamics within action potentials are likely to be determined by changes in conformational dynamics in molecular protein assemblies where memories are read, written and stored. Importantly we may understand now how changes and computations that occur at molecular level, electrical patterns that occur within spikes are related together and generate the representation of presented objects. Given that all cells respond to all stimuli and that the neural code is most likely distributed amongst many cells the statistical analysis of electrical patterns in the neuronal ensemble tell more about the whole image class. Importantly, a comparative analysis of spike directivity from all four neurons together provides a highly significant separation between categories ($F=6.09$ $p=0.0023$) while firing rate and interspike interval data do not display a statistical significant separability. This result shows that information is likely to be electrically inferred by neurons "which behave as weak learners attending to preferred spatial directions in the probably approximately correct sense" (Aur and Jog, 2007a). Additionally, in order to extract relevant information regarding presented categories from ISI and firing rate data an increased number of cells is required ($n>4$). The above results can be summarized in terms of how categories were identified, classified and activated in these neurons (Tranel et al. 1997) in a 'top-down' - 'bottom-up' framework (Figure 5). If only temporal characteristics either firing rate or ISI are considered then information regarding input categories or objects is highly compressed. Therefore, it is likely that presented images cannot be reconstructed/ remembered solely based on an existent temporal code (Figure 5,a). The selective occurrence of electrical patterns within analyzed APs demonstrates that information processing is preferentially processed and stored at molecular scale, ion channel level in different anatomical parts of analyzed neurons. Electrical micro-maps reveal better this information regarding input categories and objects. Therefore, it is likely that original images can be better reconstructed/remembered based on information embedded in electrical patterns from many neurons that respond to presented objects(Figure 5,b).

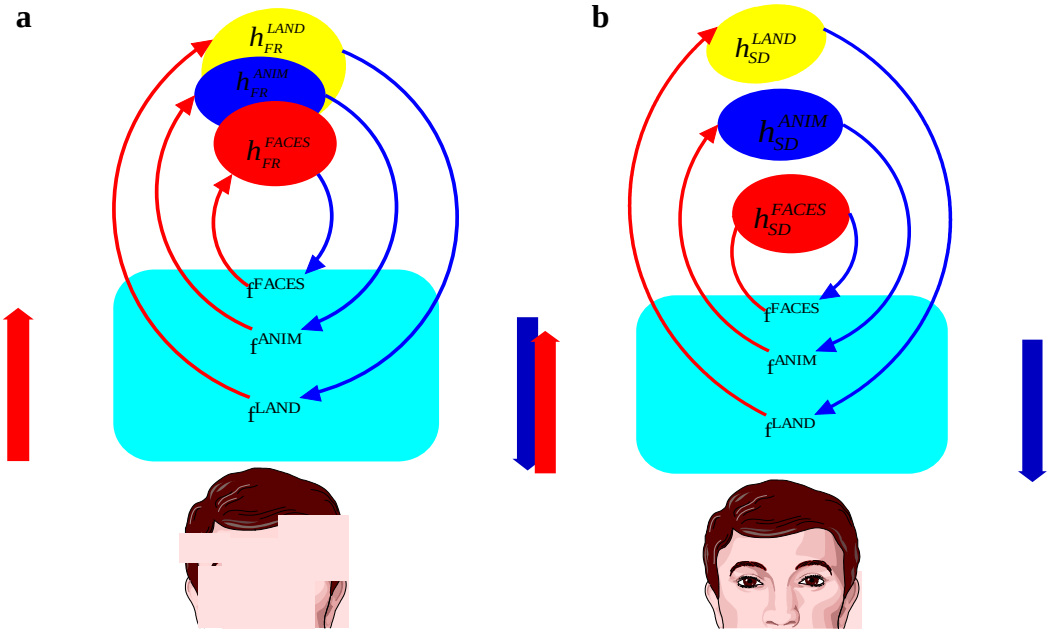

Figure 5: Schematic representation of a 'top-down', 'bottom-up' processing system in an ensemble of neurons where information is linked together

a, The original image cannot be generated if firing rate/ISI is considered from recorded cells

b, The original image is generated if electrical patterns from several neurons are considered

Spike directivities are related to synaptic and non-synaptic inputs that generate AP onset and temporal variability of APs occurrence. In order to better characterize the presented objects information should be extracted from all features including information from temporal patterns. However, these analyses reveal that fundamental aspects of information processing, communication and computation can be hidden to temporal analysis (firing rate, ISI) and raises questions regarding the richness, reliability and existence of temporal code. Indeed electrical patterns occur at a different scale within the neuron where it is likely to be determined by and generate significant molecular changes at DNA, gene or conformational alterations at protein level. This fundamental change in perceiving 'neural code' may help us to understand memory-related phenomena and theoretically connect these changes in electrical patterns with molecular machinery and complex electrochemical processes.

This new result displays the existence of an important "lower level" of coding where information is processed in a distributed parallel manner and can be modeled as a result of electric interactions and dynamics of electric charges (Aur and Jog, 2010). Using few experiments and extensive computational modeling techniques in developing *neuroelectrodynamics* we predicted that the transient charge density dynamics within a millisecond-level time domain of AP provides meaningful information. This result proves that with adequate computational methods (e.g. spike directivity) this information can be read from spikes and offers details regarding object category representation.

Additionally, we predicted that information regarding charge density, emerging electric field can be dynamically 'written in memory' within synthesized proteins and their interactions. Since quantum properties of information processing occur almost anywhere at microscopic molecular scales it is likely that these phenomena could have an influence and can be exploited in neural information processing (Hameroff and Tuszynski, 2004).

In order to experimentally test this hypothesis, the experiment requires controlling the electric field in addition to other characteristics and simultaneously record and analyze the protein response and protein–protein interactions. Given technological progress and innovations in wet labs (Blanchard, et al., 2004; Aitken and Puglisi, 2010) it has become possible to monitor in real time conformational dynamics and *w*e expect any day soon to hear that the problem was completely solved.

The propagation of action potential during a millisecond time, the charge density dynamics is not random, it is related to information processed and communicated by the neuron. Since electrical micro-maps in APs reflect encoded percepts generated in an explicit topographic manner this result demonstrates that APs are not stereotype events and cannot be reduced to binary, all or none events without loosing meaningful information. Additionally, several different features of presented images are 'read' or 'written' within these neurons and little information received synaptically and non-synaptically about a certain feature can trigger the neuron to fire. If the analysis is not restricted to short time periods the neuron will respond to other presented objects. Additionally 'abstract' information regarding one object is distributed inside several cells. Therefore the 'abstract' information needed to 'recreate' any presented object, category is a result of information inference from many electrical patterns that occur in the activity of several neurons and it is unlikely that one neuron will always respond only to Jennifer Aniston or Halle Berry and the main question remains. Where is the 'Jennifer Aniston neuron'?

References

Aitken, C.E., Puglisi, J.D. (2010)Following the intersubunit conformation of the ribosome during translation in real time,Nature Structural and Molecular Biology 17 (7), pp. 793-800,

Abbott, L.F., Varela, J.A., Sen, K., Nelson, S.B. (1997) Synaptic depression and cortical gain control Science, 275 (5297), pp. 220-224

Adrian, E. D. (1928) The basis of sensation: The action of the sense organs. New York: Norton Aur D, Jog MS, (2007a) Neuronal spatial learning, Neural Processing Letters, Vol 25, no 1, pp 31,47, http://dx.doi.org/10.1007/s11063-006-9029-2

Aur D and Jog MS, (2007b) Reading the Neural Code: What do Spikes Mean for Behavior? Nature Precedings <http://dx.doi.org/10.1038/npre.2007.61.1,

Aur D., Connolly C.I., Jog M.S., (2005) Computing spike directivity with tetrodes, Journal of Neuroscience Methods, 149 (1), pp. 57-63.

Aur D., Jog MS (2006) Building Spike Representation in Tetrodes, Journal of Neuroscience Methods, vol. 157, Issue 2, 364-373.

Aur, D. and Jog, MS., (2010) Neuroelectrodynamics, Understanding the Brain language: IOS Press.

Blanchard, S.C., Kim, H.D., Gonzalez, R.L. Jr., Puglisi, J.D. & Chu, S. (2004). Fluorescence resonance energy transfer (FRET) . tRNA dynamics on the ribosome during translation. Proc. Natl. Acad. Sci. USA 101, 12893–12898

Felleman, D.J., Van Essen, D.C. (1991) Distributed hierarchical processing in the primate cerebral cortex, Cerebral Cortex 1 (1), pp. 1-47 1864

Freedman, D.J., Miller, E.K. (2008) Neural mechanisms of visual categorization: Insights from neurophysiology Neuroscience and Biobehavioral Reviews 32 (2), pp. 311-329

Gerstner and Kistler W.M. (2002), Spiking Neuron Models - Single Neurons, Populations, Plasticity, Cambridge Univ. Press.

Gold C, Henze DA, Koch C, Buzsáki G., (2006) On the origin of the extracellular action potential waveform: amodeling study. J Neurophysiol 95: 3113-3128

Hameroff, S., Tuszynski, J., (2004) Quantum states in proteins and protein assemblies: The essence of life? Proceedings of SPIE - The International Society for Optical Engineering 5467, pp. 27-41

Honey, C.J., Kötter, R., Breakspear, M., Sporns, O. (2007) Network structure of cerebral cortex shapes functional connectivity on multiple time scales, Proceedings of the National Academy of Sciences of the United States of America 104 (24), pp. 10240-10245

Quiroga Q, , Mukamel R., , Isham R., , Malach E.A. Fried, I. (2008) Human single-neuron responses at the threshold of conscious recognition, Proceedings of the National Academy of Sciences of the United States of America 105 (9), pp. 3599-3604

Quiroga, R.Q., Reddy, L., Kreiman, G., Koch, C., Fried, I. (2005) Invariant visual representation by single neurons in the human brain Nature 435 (7045), pp. 1102-1107

Quiroga R.Q, Kraskov R., A., Koch, C., Fried, I. (2009) Explicit Encoding of Multimodal Percepts by Single Neurons in the Human Brain, Current Biology 19 (15), pp. 1308-1313

Kreiman, G., Koch, C., Fried, I. (2000) Imagery neurons in the human brain, Nature 408 (6810), pp. 357-361.

Liu, H., Agam, Y., Madsen, J.R., Kreiman, G. (2009) Timing, Timing, Timing: Fast Decoding of Object Information from Intracranial Field Potentials in Human Visual Cortex Neuron 62 (2), pp. 281-290

Shadlen, M.N., Newsome, W.T. (1998) The variable discharge of cortical neurons: Implications for connectivity, computation, and information coding, Journal of Neuroscience 18 (10), pp. 3870-3896

Shirvalkar, P.R. 2009 Hippocampal neural assemblies and conscious remembering, Journal of Neurophysiology 101 (5), pp. 2197-2200

Softky, W.R., Koch, C. (1993) The highly irregular firing of cortical cells is inconsistent with temporal integration of random EPSPs Journal of Neuroscience 13 (1), pp. 334-350.

Steinmetz, P.N. (2009) Alternate task inhibits single-neuron category-selective responses in the human hippocampus while preserving selectivity in the amygdala , Journal of Cognitive Neuroscience 21 (2), pp. 347-358

Terrell G. R. and Scott D. W. (1992)Variable kernel density estimation. The Annals of Statistics, 20(3):1236-1265,

Tranel, D., Damasio, H., Damasio, A.R. (1997) A neural basis for the retrieval of conceptual knowledge Neuropsychologia 35 (10), pp. 1319-1327.

Appendix 1

In a biological neuron action potential generation involves selective activities of ion channels. The collective properties of large ion channel ensembles can be modeled as spatial changes in

the dynamics and distribution of electric charges. Spike directivity approximates with a vector this spatial propagation of electric field in a neuron and the resulting distribution of electric charges within a millisecond time frame. If in space the origin of a recording electrode is considered the frame of reference, then the spatial distribution of electric charges can be characterized globally by their "directivity" over the selected frame of reference. The details for computing spike directivity were presented in [15]. In the first step the trajectory $d(x, y, z)$ of charge during AP propagation is computed using a Newton-Raphson algorithm:

$$d_{n+1} = d_n - J^{-1} F(d_n),\ n \in N \qquad \textbf{(9)}$$

where the signals $s_0(k)$, $s_1(k)$, $s_2(k)$ and $s_3(k)$, $k \in \mathbf{N}$ are recorded from the four nearby electrodes**:**

$$\begin{aligned} \frac{s_0(k)}{s_1(k)} &= \frac{(x(k)-x_1)^2+(y(k)-y_1)^2+(z(k)-z_1)^2}{x(k)^2+y(k)^2+z(k)^2} \\ \frac{s_0(k)}{s_2(k)} &= \frac{(x(k)-x_2)^2+(y(k)-y_2)^2+(z(k)-z_2)^2}{x(k)^2+y(k)^2+z(k)^2} \\ \frac{s_0(k)}{s_3(k)} &= \frac{(x(k)-x_3)^2+(y(k)-y_3)^2+(z(k)-z_3)^2}{x(k)^2+y(k)^2+z(k)^2} \end{aligned} \qquad \textbf{(10)}$$

and x_i,y_i,z_i i=0,3 are the positions in the space of the tips of electrodes. Spike directivity is then obtained as a linear approximation of the computed trajectory by performing a singular value decomposition (SVD) of trajectory coordinates (x(k),y(k),z(k)):

$$P = \begin{pmatrix} x(1) & y(1) & z(1) \\ \dots & \dots & \dots \\ x(n) & y(n) & z(n) \end{pmatrix} \qquad \textbf{(11)}$$

where k=1,2…,n.

$$P_{tr\ nx3} = U_{nxn} S_{nx3} V_{3x3}^{T} \qquad \textbf{(12)}$$

and V is the corresponding "right" singular vector that represents direction cosines of the best linear approximation.

Appendix 2: The set description includes all five presented images for faces f^{FACES} :

$$f^{FACES} = \{f^{Face1}, f^{Face2}, f^{Jennifer}, f^{Ander}, f^{Drew}\} \qquad \textbf{(13)}$$

five presented images for animals f^{ANIM}:

$$f^{ANIM} = \{f^{Monkey}, f^{Horse}, f^{Eleph}, f^{Spider}, f^{Tiger}\} \qquad \textbf{(14)}$$

and five presented images for landscapes f^{LAND}:

$$f^{LAND} = \{f^{Out10}, f^{Out12}, f^{Out20}, f^{Out26}, f^{Out28}\} \qquad \textbf{(15)}$$

where $f^{FACES} \in F^{FACES}$, $f^{ANIM} \in F^{ANIM}$ and $f^{OUT} \in F^{OUT}$.

The presentation of each image category generates in the output space the following sets for faces h^{FACES}

$$h^{FACES} = \{h^{Face1}, h^{Face2}, h^{Jennifer}, h^{Ander}, h^{Drew}\} \quad \textbf{(16)}$$

for animals h^{ANIM}:

$$h^{ANIM} = \{h^{Monkey}, h^{Horse}, h^{Eleph}, h^{Spider}, h^{Tiger}\} \quad \textbf{(17)}$$

and for landscapes:

$$h^{LAND} = \{h^{Out10}, h^{Out12}, h^{Out20}, h^{Out26}, h^{Out28}\} \quad \textbf{(18)}$$

where $h^{FACES} \in H^{FACES}$, $h^{ANIM} \in H^{ANIM}$ and $h^{OUT} \in H^{OUT}$.

Supplementary figures

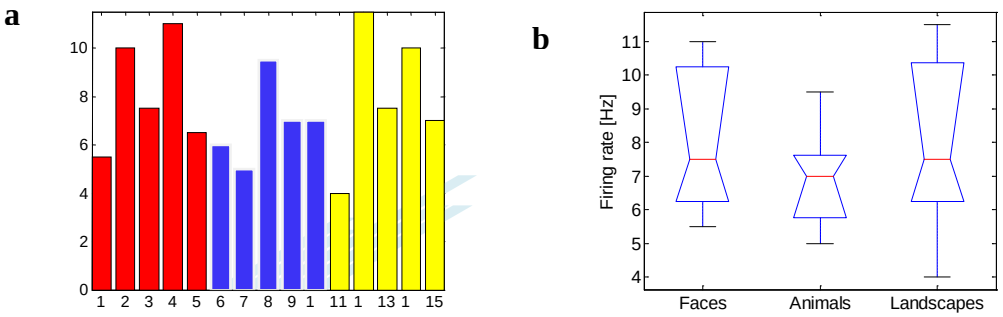

Figure 6: Example of a representative neuron where the firing rate analysis does not show significant difference between faces in red, animals in blue and landscape in red (N1, p_{FR}=0.678). The first five bars represent the characteristics of f^{FACES} and their order is specified in Eq.(4) the next five bars represent the characteristics of the five animals f^{ANIM} and their order is specified in Eq.(5) and the last five represent the characteristics of f^{LAND} in the order specified in Eq.(6). The responses are between 200 and 2,000 ms after stimulus onset.

a Mean instantaneous frequency as the median number of spikes across trials for f^{FACES}, f^{ANIM} and f^{LAND}

b, One way ANOVA for the mean instantaneous frequency data (p_{FR}=0.678)

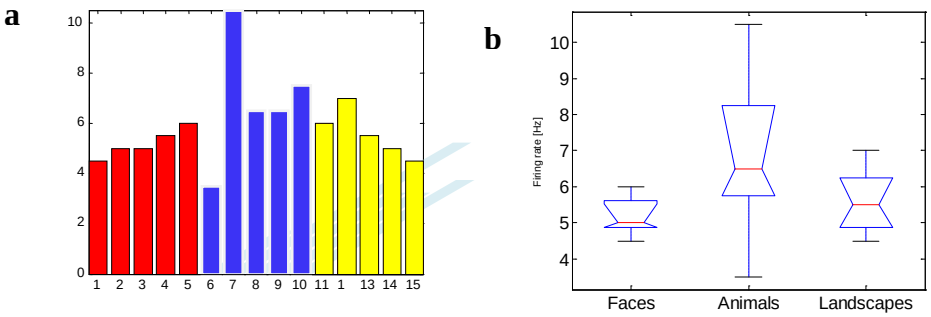

Figure 7: Representation of firing rate in red for faces , in blue for animals and in yellow for landscapes and corresponding p-values for separating these three categories in the neuron (N2 p_{FR} =0.2480)

a Mean instantaneous frequency for f^{FACES}, f^{ANIM} and f^{LAND}

b, One way ANOVA for the mean instantaneous frequency data (p_{FR} =0.2480)

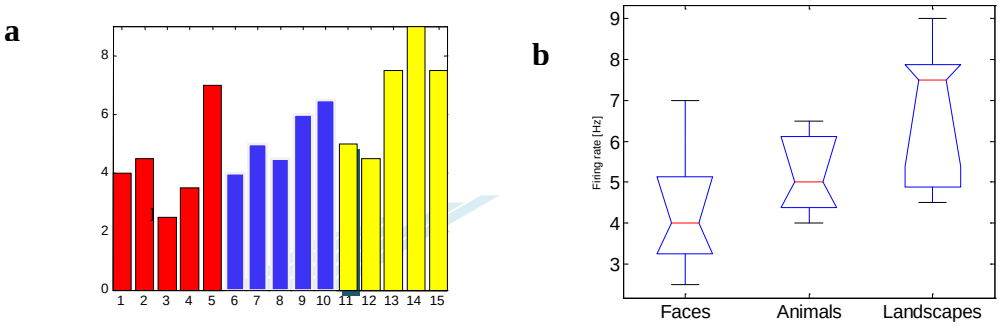

Figure 8: Representation of firing rate in red for faces, in blue for animals and in yellow for landscapes and corresponding p-values for separating these three categories in the neuron (N3 : p_{FR} =0.090)

a, Mean instantaneous frequency for f^{FACES}, f^{ANIM} and f^{LAND}

b, One way ANOVA for the mean instantaneous frequency data (p_{FR} =0.090)

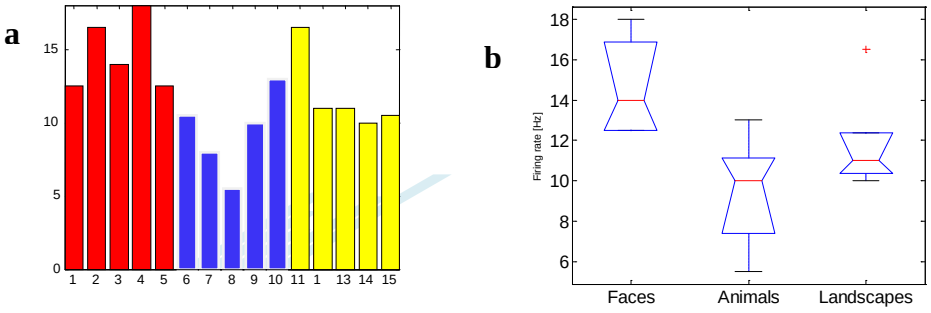

Figure 9: Representation firing rate in red for faces, in blue for animals and in yellow for landscapes and corresponding p-values for separating these three categories in the neuron (N4: p_{FR}=0.0261)

a, Mean instantaneous frequency for f^{FACES}, f^{ANIM} and f^{LAND}

b, One way ANOVA for the mean instantaneous frequency data (p_{FR}=0.0261)

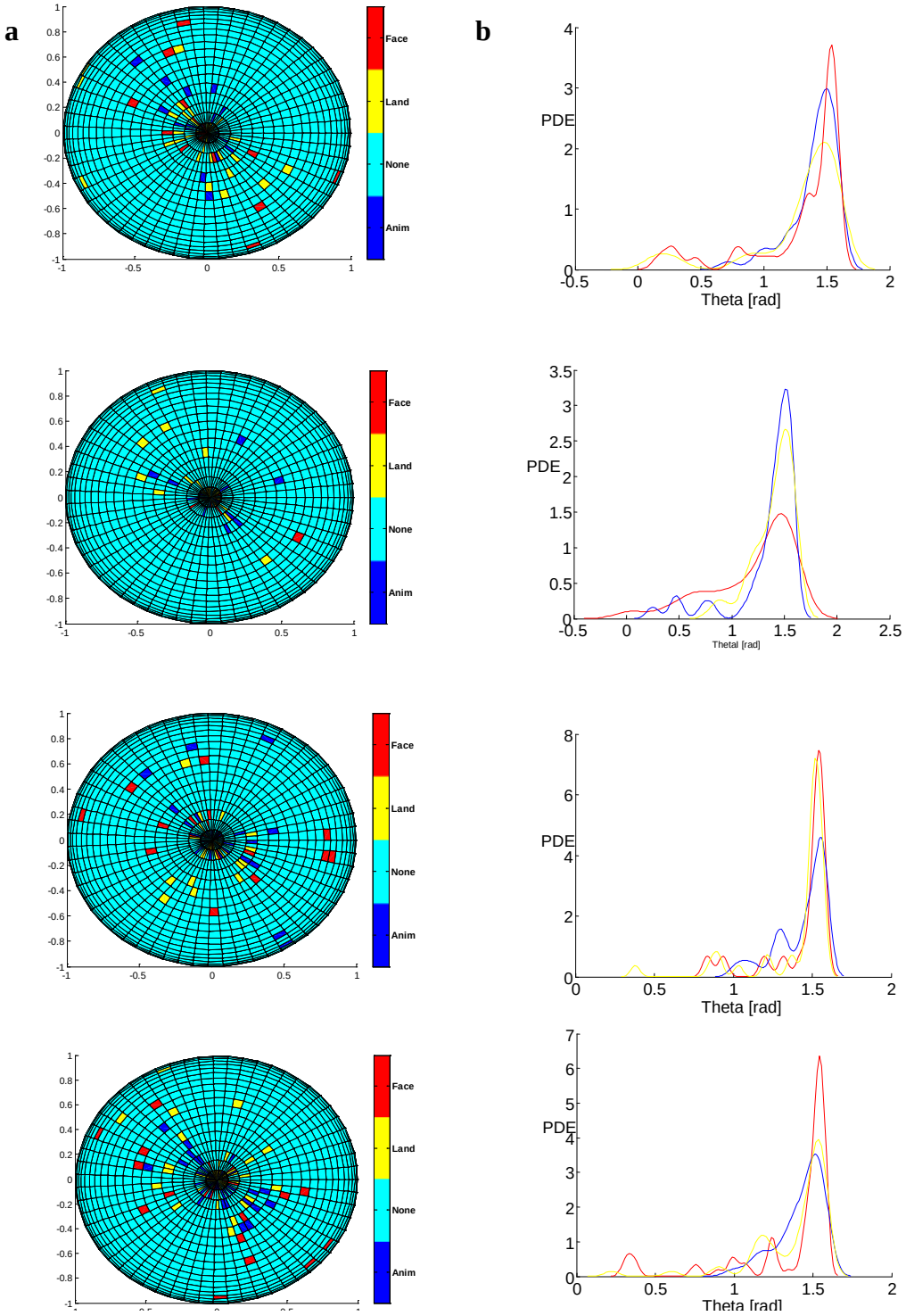

Figure 10: Representation of spike directivity features mapped on the north hemisphere in case of four analyzed neurons from MTL and the corresponding probability density estimate of the spike directivity (θ_i angles) for faces, animals and landscapes.

a. The representation of spike directivity features regarding faces in red color, animals in blue color, landscape in blue color

b. Probability density estimate of the spike directivity (θ_i angles) in selected neurons displays clustering effect (faces in red color, animals in blue color, landscape in blue color)

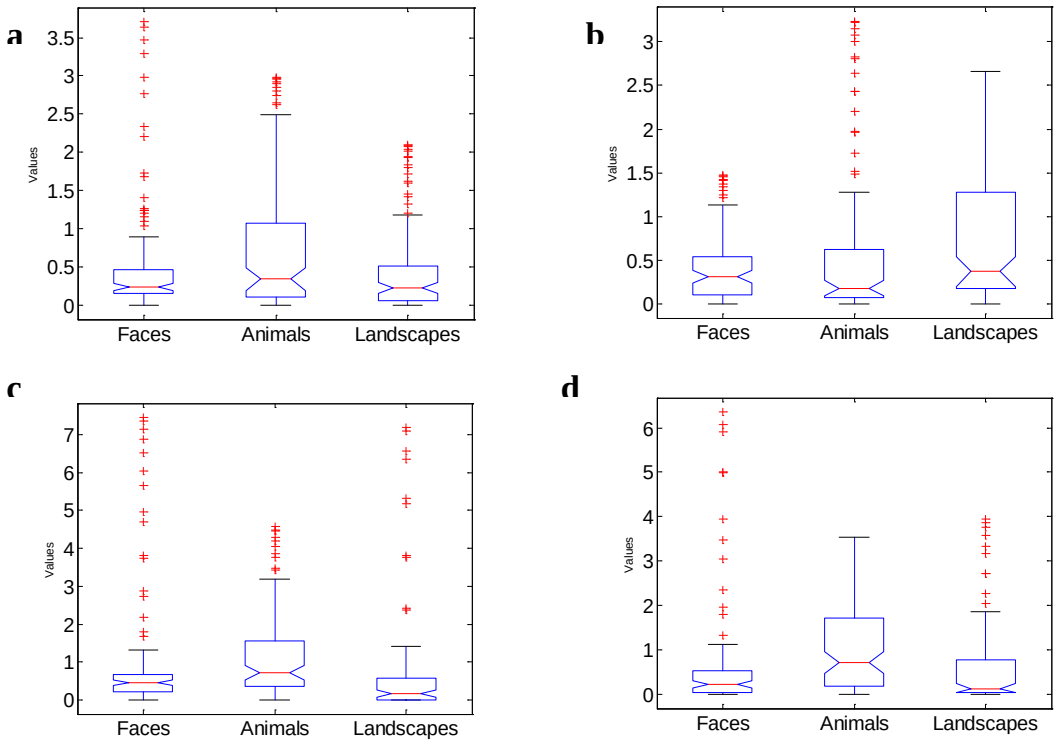

Figure 11: One way ANOVA analysis of probability density estimate of spike directivity (θ_i angles) from north hemisphere shows that the difference between categories (face and animal, landscape) is significant in three neurons and marginally significant for the fourth neuron. a, One way ANOVA for the neuron N1 shows significant difference in case of f^{FACES} ,animals f^{ANIM} and landscapes f^{LAND} (p_{SD}^{N} =0.028); b, One way ANOVA for the neuron N2 shows highly significant difference in case of f^{FACES} ,animals f^{ANIM} and landscapes f^{LAND} , p_{SD}^{N} =0.0012 c, One way ANOVA for the neuron N3 displays marginally significant difference in case of f^{FACES} ,animals f^{ANIM} and landscapes f^{LAND} (p_{SD}^{N} =0.065<0.1); d, One way ANOVA for the neuron N4 shows significant difference in case of f^{FACES} ,animals f^{ANIM} and landscapes f^{LAND} (p_{SD}^{N} =0.011)

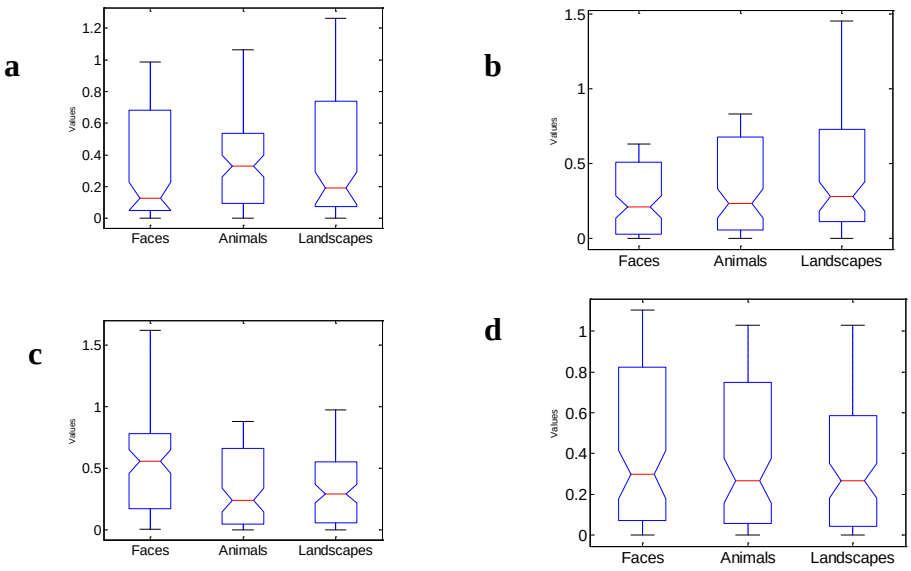

Figure 12: One way ANOVA analysis of probability distribution of ISI displays high category separability in two neurons N1 and N3

a, One way ANOVA for the probability distribution of ISI in N1; p_{ISI} =0.3196

b, One way ANOVA for the probability distribution of ISI in N2; p_{ISI} =0.0008

c, One way ANOVA for the probability distribution of ISI in N3; p_{ISI} = 9.9749e-007

d, One way ANOVA for the probability distribution of ISI in N4: p_{ISI} = 0.1723

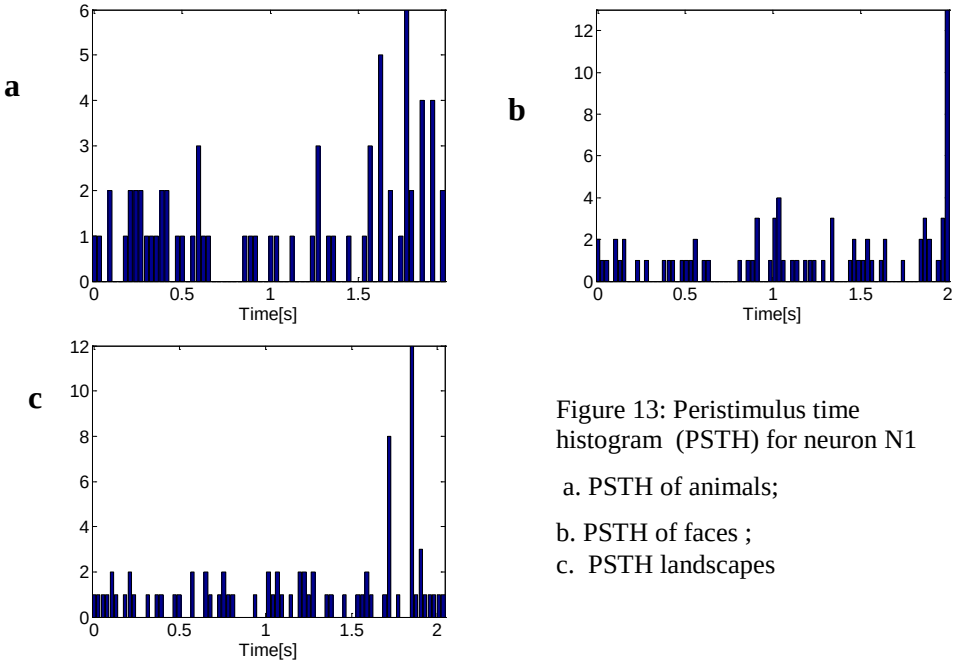

Figure 13: Peristimulus time histogram (PSTH) for neuron N1

a. PSTH of animals;

b. PSTH of faces ;

c. PSTH landscapes

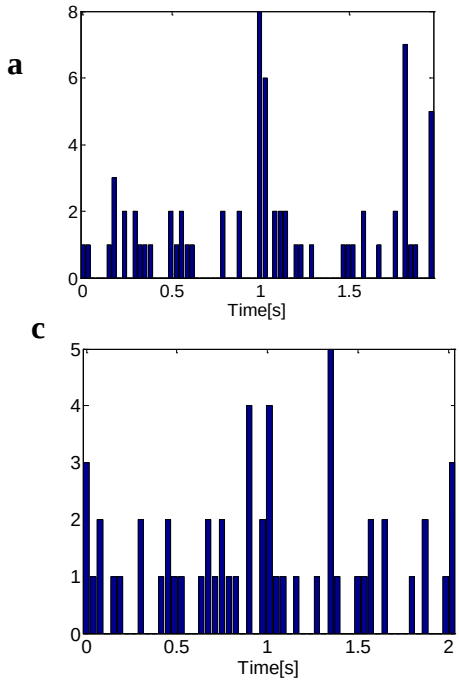

Figure 14: Peristimulus time histogram for neuron N2

a. PSTH of animals;
b. PSTH of faces
c. PSTH landscapes

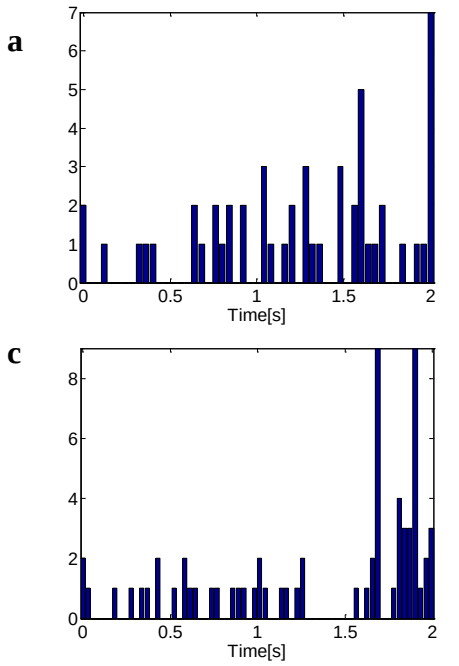

Figure 15: Peristimulus time histogram (PSTH) for neuron N3

a. PSTH of animals;
b. PSTH of faces
c. PSTH landscapes

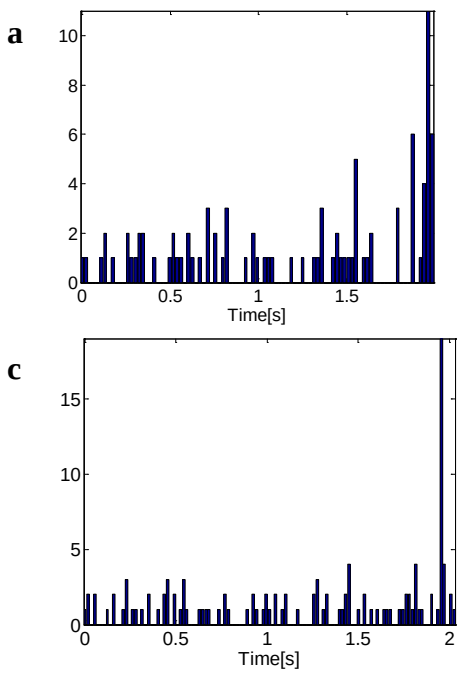

Figure 16: Peristimulus time histogram for neuron N4

a. PSTH of animals;
b. PSTH of faces
c. PSTH landscapes

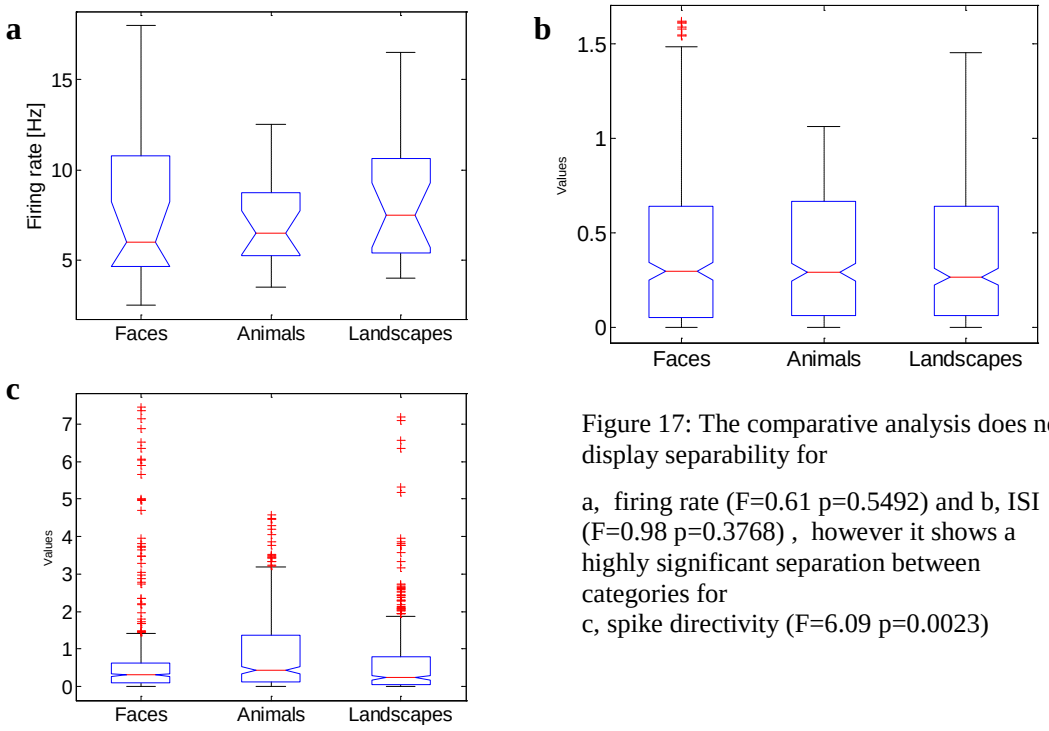

Figure 17: The comparative analysis does not display separability for

a, firing rate (F=0.61 p=0.5492) and b, ISI (F=0.98 p=0.3768) , however it shows a highly significant separation between categories for
c, spike directivity (F=6.09 p=0.0023)

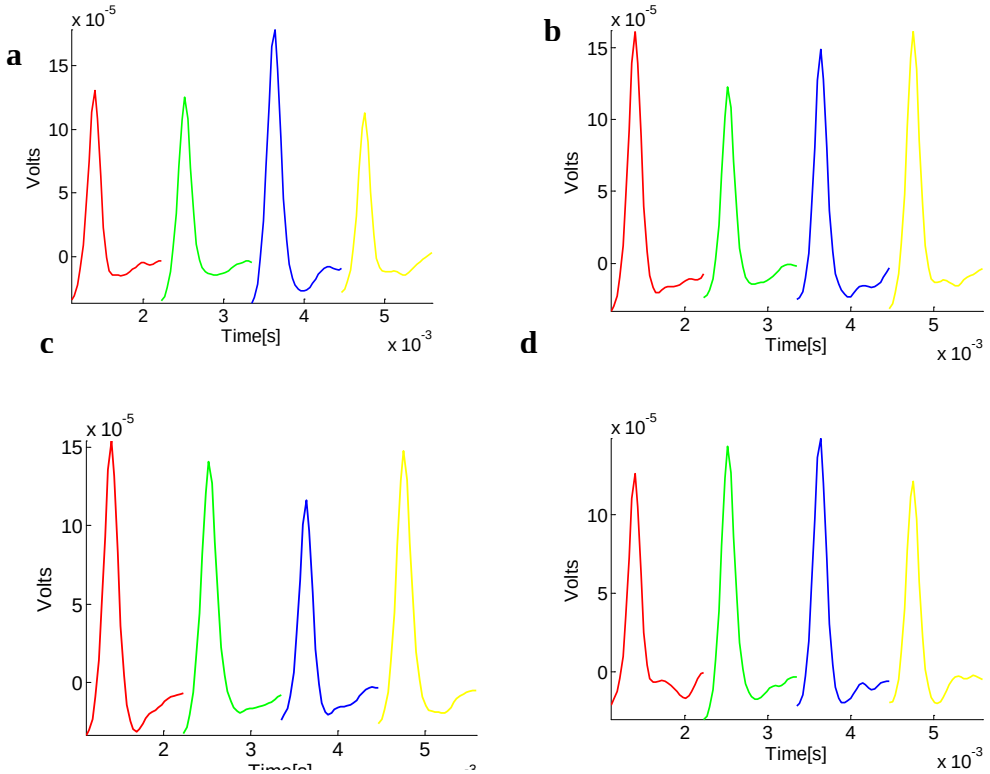

Figure 18: The mean amplitudes of waveforms recorded from four neurons a, N1, b. N2, c. N3 and d. N4

	Channel 1	Channel 2	Channel 4	Channel 4
N1	0.1302	0.1250	0.1777	0.1613
N2	0.1616	0.1228	0.1491	0.1613
N3	0.1542	0.1407	0.1161	0.1477
N4	0.1264	0.1437	0.1484	0.1215

Table 2: The maximum values for the means of amplitudes for all 4 selected neurons